V European Conference on Computational Fluid Dynamics
ECCOMAS CFD 2010
J. C. F. Pereira and A. Sequeira (Eds)
Lisbon, Portugal,14-17 June 2010

NUMERICAL SIMULATION OF THE FLUID-STRUCTURE INTERACTION IN STENTED ANEURYSMS.

Joaquín Mura, Miguel A. Fernández and Jean-Frédéric Gerbeau

INRIA Paris - Rocquencourt
REO Team,
Domaine de Voluceau, Rocquencourt - B.P. 105
78153 Le Chesnay cedex, France.
e-mail: {joaquin.mura,miguel.fernandez,jean-frederic.gerbeau}@inria.fr

Key words: Fluid-structure interaction, Robin-Neumann boundary conditions, Hemodynamics, Enclosed fluid problems

Abstract. *An aneurysm is a pathological condition whereby a weakened artery wall may dilates up to dangerous proportions. One of the most common treatments consists of the insertion of a stent graft, which is a medical device introduced into the artery lumen in order to diminish the pressure on the aneurysm wall and so avoiding its rupture.*

In this article we perform the simulation of the fluid-structure interaction between the blood, the artery wall and the stent. We consider the blood modeled by incompressible Navier-Stokes equations in ALE formulation, while the solid parts are modeled using non-linear shells in a Lagrangian framework. We suppose the stent being perfectly matched with the artery, i.e., with no filtrations or endoleaks, such that we obtain two disconnected regions of fluid by the stent wall.

The main difficulty in this problem is the numerical solution for the isolated portion of fluid, where the explicit coupling with standard Dirichlet-Neumann boundary conditions may lead to non uniqueness for the intra-aneurysm pressure and also to violate the divergence free condition. To address this issue we use Robin-Neumann conditions for the coupling, which allow us not only to obtain successful numerical simulations but also a less sensitive scheme to the added-mass effect and a more stable and robust iterative technique than the Dirichlet-Neumann procedure.

We present numerical evidence of the well-posedeness of this technique and examples showing the effect of the stent on the aneurysm wall.

1 INTRODUCTION

The aortic aneurysm is a bulbous enlargement of the aorta that eventually may burst. Among the different types of aortic aneurysms the most common is the abdominal one (AAA), present in approximately 5%-7% of people over the age of 60 (see e.g. [6]). Even though the AAA rupture represents an important cardiovascular risk, a completely reliable technique to predict its behavior is not yet available [10]. To improve and simplify the follow-up of AAA, a device allowing the remote monitoring of the pressure is currently in development [8]. The computer simulations presented in this work are a first step to contribute to this emerging technique.

This work aims at the numerical simulation of stented AAA, where two fluid-structure interaction problems have to be worked out: the artery-blood flow and stent graft-blood flow. To address it, we focus on partitioned algorithms, i.e., one solver for the fluid and another one for the solid, whose main advantage lies in the fact that the fluid and the solid can be solved separately, reusing some existing code and giving the possibility of parallelize resources. The classical strategy to enforce the continuity in velocity and surface tension at the interfaces is to solve the FSI through the Dirichlet-Neumann approach, but in this case, however, the direct imposition of displacement conditions on the interface may be inconsistent with the divergence-free condition in the fluid region enclosed by elastic walls.

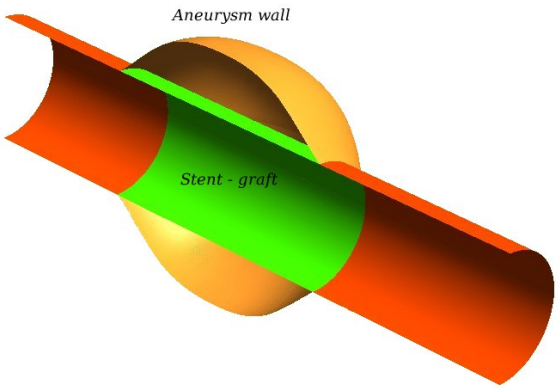

Figure 1: Simplified scheme with description of the geometry: Half artery view and its solid walls.

Instead of using standard coupling conditions at the interface, that could make difficult the computations in the case of multiple interacting surfaces, our strategy follows that of [3], where a Robin-Neumann interface condition (RN) is introduced, namely, Robin in the fluid side and Neumann in the solid one. As reported in [1, 3], the RN shows good convergence properties and insensitivity with respect to the added-mass effect, which plays a fundamental role in the simulation of blood flow in arteries.

The outline of the paper is as follows. In section 2 we introduce the mathematical model of the FSI. In section 3 an algorithm is presented to solve numerically the FSI problem through the Robin-Neumann interface condition. Section 4 is devoted to some numerical examples and finally, some remarks and final comments in the section 5.

2 GOVERNING EQUATIONS

The nonlinear fluid-structure model follows [5, 3], whereby we consider the fluid-solid domain composed by $\Omega(t) = \Omega^f(t) \cup \Omega^s(t)$, whose fluid region is contained in $\Omega^f(t)$ and the solid in $\Omega^s(t)$, both depending on time t. The outgoing normal vector to the solid domain is n^s, while for the fluid is n^f. The surface where the interaction occurs will be denoted by $\Sigma(t) = \overline{\partial\Omega^f(t)} \cap \overline{\partial\Omega^s(t)}$.

2.1 Structure model

In a Lagrangian framework, the variables in the solid are defined in the reference domain $\hat{\Omega}^s = \Omega^s(0)$. We will denote the quantities with the hat symbol $\hat{\cdot}$ when they are associated to that fixed domain. The deformation at time t is described through the deformation field $\varphi : \hat{\Omega}^s \times (0,T) \to \Omega(t)$, $T > 0$ being a finite bound in time. The deformation gradient is $F^s = I + \nabla_{\hat{x}}\varphi$ and its jacobian $J^s = detF^s$. The boundary of the solid body is composed by $\partial\hat{\Omega}^s = \hat{\Sigma} \cup \hat{\Gamma}_d \cup \hat{\Gamma}_n$, with Γ_d and $\hat{\Gamma}_n$ denotes the Dirichlet (clamped) and the Neumann (stress-free) boundary, respectively.

The displacement of the solid d is obtained by solving the following system in a Lagrangian framework:

$$\left.\begin{array}{rcll} \rho^s\partial_{tt}d - \mathrm{div}\left(J^s\sigma^s(d)(F^f)^{-T}\right) &=& 0 & \text{in } \hat{\Omega}^s, \\ d &=& 0 & \text{on } \hat{\Gamma}_d, \\ J^s\sigma^s(d)(F^f)^{-T}n^s &=& 0 & \text{on } \hat{\Gamma}_n, \\ \partial_t d(\cdot,0) &=& 0 & \text{in } \hat{\Omega}^s, \end{array}\right\} \tag{1}$$

where ρ^s represents the density of the solid and σ^s the Cauchy stress tensor.

2.2 Fluid model

For the fluid, we consider the Navier-Stokes equations in ALE formulation. For the sake of simplicity, we write down the equations with pressure-type boundary conditions through $\bar{p}$:

$$\left.\begin{array}{rcll} \rho^f\partial_t u + (u-w)\cdot\nabla u - \mathrm{div}\sigma^f(u,p) &=& 0 & \text{in } \Omega^f(t), \\ \mathrm{div}u &=& 0 & \text{in } \Omega^f(t), \\ \sigma^f(u,p)n^f &=& -\bar{p}n^f & \text{on } \Gamma, \end{array}\right\} \tag{2}$$

where ρ^f denotes the density of the fluid, u is the velocity and p the pressure. The term σ^f represents the Cauchy stress tensor for the fluid having the form $\sigma^f(u,p) =$

$-pI + 2\mu e(u)$ and $e(u) = \frac{1}{2}(\nabla u + (\nabla u)^T)$, μ being the viscosity of the fluid. The field w corresponds to the fluid domain velocity, obtained as an harmonic extension from the solid to the fluid domain via solving the homogeneous Laplace problem with $w = \partial_t d$ as boundary condition on Σ. We introduce the displacement of the fluid domain obtained by the extension operator Ext: $L^2(\Sigma) \to H^1(\Omega^f)^3$ (that represents the harmonic extension mentioned above), such that $d^f :=\text{Ext}(d|_{\hat{\Sigma}})$. With this, we can write $w = \partial_t d^f$ in Ω^f.

2.3 Coupling conditions

In the continuous level, the coupling between the solid and the fluid concerns the continuity of velocity and equilibrium of forces through the interface, i.e., the quantities d, u, p, σ^s and σ^f must satisfy

$$u = \partial_t d, \tag{3}$$
$$\sigma^s(d)n^s + \sigma^f(u,p)n^f = 0, \tag{4}$$

on $\Sigma(t)$ for any time $t \in (0,T)$.

The RN interface boundary condition consists of a combination of the condition (3) and (4), which reads

$$u + \tilde{\alpha}\sigma^f(u,p)n^f = \partial_t d - \tilde{\alpha}\sigma^s(d)n^s \text{ on } \Sigma(t), \tag{5}$$

then (3) is replaced with (5). The constant parameter $\tilde{\alpha}$ plays the role of compliance of the solid, relaxing the condition (3) during the sub-iterations. This permits the simultaneous evaluation of velocities and stresses across the interface, enabling the solver to balance the efforts in order to satisfy some displacement restrictions, and viceversa, which is crucial in the assessment of pressure and volume preservation in the case of enclosed fluids.

3 ALGORITHM

In the sequel, the time step is denoted by $\tau > 0$, the time derivative is approximated through the backward Euler finite difference $D_\tau v^n := (v^n - v^{n-1})/\tau$. For further details on the algorithm and discretization presented here, we refer to [3] and [4].

We assume that $\Omega^{f,n}$, $\Omega^{s,n}$, (u^n, p^n) and d^n are known at the time $t = t^n$, then the computation at the new time step $n+1$ is obtained by solving

1. Fluid domain update:

$$d^{f,n+1} = \text{Ext}(d^n|_\Sigma), \quad w^{n+1} = D_\tau d^{f,n+1} \text{ in } \Omega^{f,n}, \quad \Omega^{f,n+1} := (I + d^{f,n+1}) \circ \Omega^{f,n}.$$

where d^f is the displacement associated to the fluid domain, as mentioned in section 2.2.

2. Implicit step: We define $V := H^1_\Sigma(\Omega^f)^3 \times L^2(\Omega^f) \times L^2(\Sigma)^3$ and the operator

$$F : H^1(\Omega^f)^3 \times L^2(\Omega^f) \times L^2(\Sigma)^3 \to V'$$

related with the variational formulation of (2) in order to find its solution at the time step $n+1$:

$$\begin{aligned}\langle F(u,p,\lambda),(v,q,\xi)\rangle_{V,V'} := \quad & \frac{\rho^f}{\tau}\left(\int_{\Omega^{f,n+1}} u\cdot v\,dx - \int_{\Omega^{f,n}} u\cdot v\,dx\right)\\ & -\rho^f\int_{\Omega^{f,n+1}} (\mathrm{div} w^{n+1})u\cdot v + ((u^n - w^{n+1})\cdot\nabla)u\cdot v\,dx\\ & +\int_{\Omega^{f,n+1}} \sigma(u,p) : e(v) \;+\; q\mathrm{div} u\,dx\\ & +\int_\Sigma \left(u - \frac{1}{\tau}(\lambda - d^n)\right)\cdot\xi\,ds + \int_\Gamma \bar{p}v\cdot n^f\,ds.\end{aligned} \tag{6}$$

For the structure sub-problem we introduce, formally, the Neumann-to-Dirichlet operator S such that, given the pair $(u,p) \in H^1(\Omega^f)^3 \times L^2(\Omega^f)$ solution to the fluid problem (2), yields

$$d|_\Sigma = S(u,p)$$

by solving (1). The FSI is now expressed via the relation $\lambda = S(u,p)$.

The strategy to solve the problem

$$R(u,p) = F(u,p,S(u,p)) = 0 \quad \text{in } V' \tag{7}$$

by preconditioning the fluid solver is introduced in [3], which exhibits less sensitivity to the added-mass effect than the standard DN. The idea is to improve the convergence of a fixed point algorithm to solve (7) by introducing a simplified structure solver $\tilde{S}(u,p)$, whose associated residual is

$$\tilde{R}(u,p) = F(u,p,\tilde{S}(u,p)).$$

Now, in order to find (u,p) such that $R(u,p) = 0$, we consider fixed point iterations between the fluid and the structure indexed by k, following defect-correction (or preconditioned) iterations: Given $d_{k+1} = S(u_k,p_k)$, find (u_{k+1},p_{k+1}) such that

$$\tilde{R}(u_{k+1},p_{k+1}) = \tilde{R}(u_k,p_k) - R(u_k,p_k), \tag{8}$$

which yields

$$F(u_{k+1},p_{k+1},\tilde{S}(u_{k+1},p_{k+1})) = F(u_k,p_k,\tilde{S}(u_k,p_k)) - F(u_k,p_k,S(u_k,p_k)).$$

This implies that

$$\langle \tilde{R}(u_{k+1}, p_{k+1}), (v, q, \xi) \rangle_{V,V'} = \int_{\Sigma^{n+1}} \frac{1}{\tau} \left(\tilde{S}(u_k, p_k) - S(u_k, p_k) \right) \cdot \xi \, ds,$$

for all $(v, q, \xi) \in V$. One can observe that the preconditioned residual depends on the misfit between the complete solver and the simplified one evaluated only on the interface. A good choice for this simplified solid operator is $\tilde{S} = -\alpha \sigma^f(u, p) n^f$. Using this one can obtain (see [3] for further details) that the equation (8) leads to the following coupling conditions on Σ^{n+1}:

$$\begin{aligned} \sigma^s(d_{k+1}) n^s &= -\sigma^f(u_k, p_k^n) n^f, \\ \sigma^f(u_{k+1}, p_{k+1}) n^f + \frac{\tau}{\alpha} u_{k+1} &= \frac{\tau}{\alpha} \frac{d_{k+1} - d^n}{\tau} + \sigma^f(u_k, p_k) n^f. \end{aligned} \tag{9}$$

In the equation above, α/τ is identified with $\tilde{\alpha}$ Robin-Neumann boundary condition (5). We can see this parameter as a penalization, enforcing the continuity in velocity across the interface (kinematic condition) if α is small.

4 NUMERICAL RESULTS

In order to test the effect of the stent on an artery, we select the simplified geometry shown in figure 1. The geometry of the aneurysm has of length $8[cm]$ having a radius $R = 2[cm]$ while the healthy artery radius is $R_0 = 1.0[cm]$. The mesh has 10206 nodes, where 1000 of them are lying on the stent-graft and other 1000 on the aneurysm wall. We set the Young modulus for the aneurysm wall $E_{wall} = 1.2[MPa]$ and Poisson ratio $\nu = 0.5$. For the stent we have $E_{stent} = 10[MPa]$ and $\nu = 0.27$. The thickness of the stent is $0.15[mm]$ and that of the aneurysm wall is $1.5[mm]$. The density of the fluid is $\rho^f = 1[g/cm^3]$ and that of the solid $\rho^s_{wall} = 1.12[g/cm^3]$ and $\rho^s_{stent} = 6.0[g/cm^3]$. The time step size is set to $\tau = 2 \times 10^{-3}$.

The boundary conditions consider the velocity profile at the inlet as shown in figure 2 and three-element Windkessel model at the outlet.

The structure problem is solved using MIT4 quadrilateral shells while the fluid is solved with $P_1 - P_1$ stabilized finite elements in a tetrahedral mesh (see for example [4]). To impose continuity in velocity and jump in pressure across the stent structure we follow [2], where this interface is unfolded creating two portions of fluids communicated through the stent.

4.1 Some numerical properties

To start with, we consider a test case which is not relevant from the physiological point of view, but allows to assess some numerical properties. More precisely, we clamp the aneurysm wall and observe the behavior of the stent as shown in figure 3. The numerical difficulty related with the intrasac incompressibility constraint (as pointed out in [9]) is tackled here by imposing a relaxation in the intrasac volume through (9). Therefore,

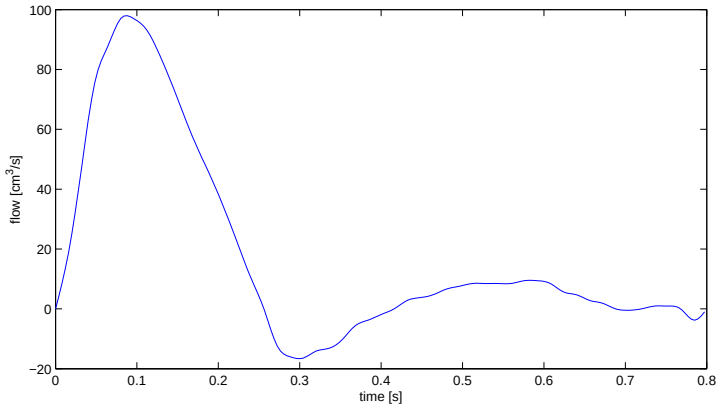

Figure 2: Flow at inlet.

the kinematic condition is achieved by minimizing the mismatch in the velocity at the interface when we solve the fixed-point iterations between the fluid and structure solvers. This technique permits to preserve the volume with a very good tolerance, as shown in 4 (less than 1% of relative error).

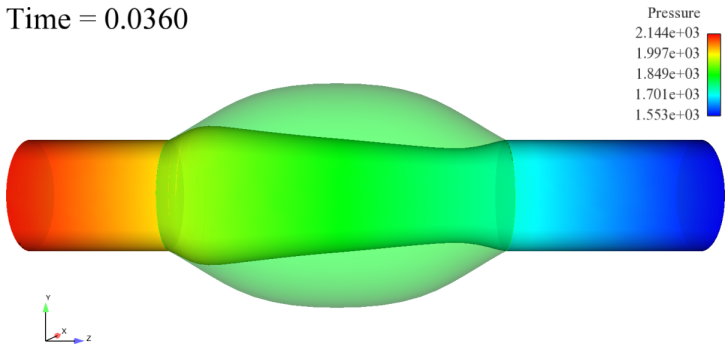

Figure 3: Clamped aneurysm wall test: Deformation of the stent-graft (×2500). The flux goes from left to right.

As reported in [1, 3], there exists a compromise between α and the convergence rate: the larger the value of α, the faster the convergence in solving (8), however, the kinematic condition is deprecated, needing more fluid-structure iterations to achieve a given tolerance. For example, in this test, to get a residual less than 10^{-7}, there were needed about 5 up to 10 FSI iterations when $\alpha = 10^{-7}$, with $\alpha = 10^{-8}$ about 15-22 iterations, but having $\alpha = 10^{-9}$ one can get more than 50 iterations. Numerical tests indicates that a good choice is, in this test, closer to $\alpha = 10^{-8}$.

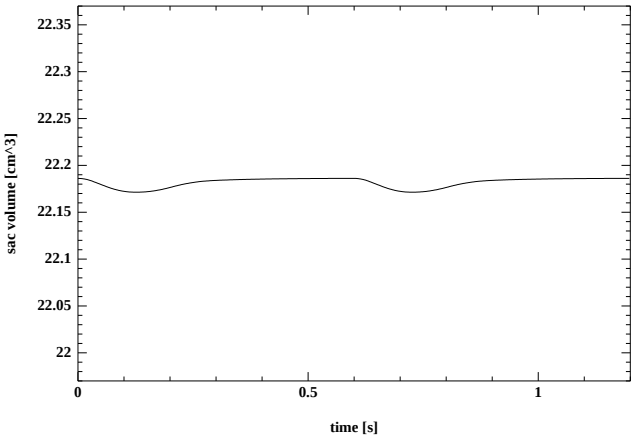

Figure 4: Evolution of the intrasac volume.

4.2 Effect of the stent-graft

The effect of the stent is presented in this preliminary result, as observed in figure 5, where both aneurysm wall and stent are elastic structures with the parameters mentioned above. To run the simulation with and without stent, firstly setting the basal pressure to zero and secondly lifting it up to 53.3$[kdyn/cm^2]$ (40$[mmHg]$), regardless the pre-stress in the artery as a first order approach.

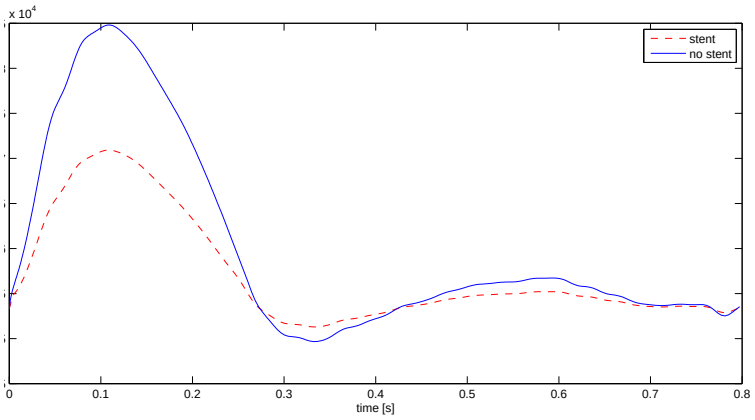

Figure 5: Maximal pressure on the aneurysm wall: Comparing the effect of the stent.

The stent helps to bear the artery pressure. The peak is 84.8$[kdyn/cm^2]$ in the case without stent-graft, while in the presence of stent we have 70.9$[kdyn/cm^2]$, this is about the half of the peak pressure without stent measuring from the basal pressure.

5 CONCLUSIONS

We have shown in this work a the Robin-Neumann algorithm can successfully solve problems with enclosed fluids (also called ballon-type problems). Moreover, it efficiently handle the added-mass effect, that degrades the performance of most of fluid-structure algorithm. However its convergence rate is sensitive to the choice of α as reported in [1, 3].

The simulations confirm that in presence of the stent the intra-sac pressure is diminished. This technique can also be used to simulate the interaction between intraluminal thrombus and stent-graft, which will be investigated in a future work.

6 ACKNOWLEDGMENTS

This work has been supported by the project ENDOCOM, funded by the national research agency (ANR), program TECSAN 2007 (http://www.endocom.upmc.fr/).

REFERENCES

[1] S. Badia, F. Nobile, C. Vergara. Fluid-structure partitioned procedures based on Robin transmission conditions. *J. Comput. Phys.*, **227** 7027–7051 (2008).

[2] M.A. Fernández, J.-F. Gerbeau and V. Martin. Numerical simulation of blood flows through a porous interface. *M2AN Math. Model. Numer. Anal.*, **42** 961-990 (2008).

[3] M.A. Fernández, Y. Maday and J. Mullaert. On the preconditioning of partitioned semi-implicit fluid-structure coupling, *Preprint.*

[4] L. Formaggia, A. Quarteroni and A. Veneziani, editors. Modeling, Simulation and Applications, **Vol. 1** Cardiovascular Mathematics. Modeling and simulation of the circulatory system.*Springer* (2009).

[5] J.-F. Gerbeau and M. Vidrascu. A quasi-Newton algorithm based on a reduced model for fluid-structure interactions problems in blood flows, *Math. Model. Num. Anal.*, **37**(4) 631–648 (2003).

[6] C. Kleinstreuer, Z. Li and M.A. Farber. Fluid-structure interaction analyses of stented Abdominal aortic aneurysms. *Annu. Rev. Biomed. Eng.*, **9** 169–204 (2007).

[7] M. Gawenda, S. Winter, G. Jaschke, G. Wassmer, and J. Brunkwall. Endotension is Influenced by Aneurysm Volume: Experimental Findings. *J. Endovasc. Therapy*, **10** 1091–1096 (2003).

[8] J. Mazeyrat, O. Romain, D. Lautru, et al. Endocom: a wireless endoprosthesis dedicated to the follow-up of abdominal aortic aneurysms, *Int. J. Artificial Organs*, **32**(7), 411-411 (2009).

[9] B. Wolters, M. Rutten, G. Schurink and F. van de Vosse. Computational modelling of endoleak after endovascular repair of abdominal aortic aneurysms, *Int. J. Numer. Meth. Biomed. Engng.* **26** 322–335 (2010).

[10] D. Vorp. Biomechanics of abdominal aortic aneurysm. *J. Biomech.*, **40** 1887–1902 (2007).